Tracking photodegradation products and bond-cleavage reaction pathways of triclosan using ultra-high resolution mass spectrometry and stable carbon isotope analysis

(Article begins on next page)

14 December 2021

Tracking toxic photodegradation products and bond-cleavage reaction pathways of triclosan using ultra-high resolution mass spectrometry and stable carbon isotope analysis

Yi Liu[1,2], Majda Mekic[1,2], Luca Carena[3], Davide Vione[3,] Sasho Gligorovski[1],Gan Zhang[1], Biao Jin[*,1]

[1] *State Key Laboratory of Organic Geochemistry, Guangzhou Institute of Geochemistry, Chinese Academy of Sciences, Guangzhou 510640, China*

[2] *University of Chinese Academy of Sciences, Beijing 10069, China*

[3] *Department of Chemistry, University of Torino, Via Pietro Giuria 5, 10125 Torino, Italy*

Submitted to *Environmental Pollution*

The first two authors contributed equally

*Corresponding author: Biao Jin (jinbiao@gig.ac.cn)

Abstract

Triclosan (TCS) is an antimicrobial compound ubiquitously found in surface waters throughout the world. Although several studies have focused on the photochemical degradation of TCS, there is still limited knowledge about its environmental fate. In this study, we got molecular-level insights into the photochemical degradation of TCS. Significant stable carbon isotope fractionation was observed during photodegradation; different bond-cleavage reaction pathways under different photolytic conditions were characterized, using compound specific isotope analysis (CSIA). Photochemical modeling of TCS photodegradation showed that direct photolysis would be the main transformation pathway if pH > 7, even in presence of dissolved organic matter. Moreover, by use of ultrahigh resolution mass spectrometry, FT-ICR-MS, a broad and complex spectrum of organic by-products (some of which potentially toxic, as assessed by a quantitative structure-activity relationship approach) were identified. A detailed reaction mechanism was developed on the basis of the detected compounds.

Capsule: TCS photo-transformation products were identified, and the concurrent bond-cleavage reaction pathways under different photolytic conditions were characterized.

1. Introduction

Triclosan (TCS) is an antimicrobial compound highly used in many common domestic products, including liquid and bar soaps, toothpaste, bathing foams and several detergents. As a high-volume household chemical, TCS is often found in wastewater treatment plants (WWTPs) and is ubiquitously spread in surface waters as well. Indeed, WWTPs do not achieve total removal and TCS is thus detected in rivers and streams at trace levels (Gautam et al., 2014; Zhao et al., 2013), with concentrations as high as 8×10^{-9} mol L^{-1} (Kolpin et al., 2002). In lakes and rivers TCS can undergo photochemical transformation by both direct photolysis and indirect photolytic processes. The former is operational when TCS absorbs sunlight, reaches excited molecular states and undergoes chemical transformation as a consequence. In contrast, indirect photochemistry is generally accounted for by the production of reactive transient species upon sunlight absorption by photosensitizers, the main one being the naturally occurring chromophoric dissolved organic matter (CDOM). Light absorption by CDOM triggers the formation of both excited triplet states (^{3}CDOM*) and reactive oxygen species (ROS), such as hydroxyl radicals ($^\bullet$OH) and singlet oxygen (^{1}O$_2$), which are able to react with TCS (Bianco et al., 2015).

The direct photolysis of TCS has been shown to be an important transformation pathway leading to the formation of diverse potentially toxic compounds (Buth et al., 2011; Sanchez-Prado et al., 2006), especially as far as the basic (anionic) TCS form is concerned (Bianco et al., 2015). The photodegradation of TCS is affected by humic acid (HA), which is an important fraction of the dissolved organic matter (DOM), and adds to the complexity of the

photochemistry conundrum (Vione and Scozzaro, 2019). Under irradiation, HA is able to generate a number of reactive transients such as ROS, triplet states, solvated electrons, and carbon-centered radicals (Aiken et al., 2011; al Housari et al., 2010; Holder-Sandrik, 2000; Zhang et al., 2011), which might be involved in TCS indirect phototransformation. However, despite an important number of studies focused on the photolysis rates and degradation products of TCS, several aspects of these processes are still unknown.

Compound specific isotope analysis (CSIA) is a powerful tool to prove the occurrence of degradation processes as well as to elucidate bond-cleavage reaction pathways of organic contaminants (Hofstetter et al., 2008; Schmidt and Jochmann, 2012). This novel approach is based on the fact that, during a reaction following normal isotopic effects, light isotopes at reactive positions are preferentially consumed compared with the heavy ones. The advantage of the CSIA method is to identify reaction pathways by analyzing the isotopic composition of the parent compounds. So far, carbon has been the most frequently applied element for CSIA applications. Carbon-based CSIA has been applied to characterize biotic and abiotic reactions for a wide spectrum of organic contaminants, including chlorinated solvents (Blessing et al., 2009; Buchner et al., 2017; Sherwood Lollar et al., 2001), BTEX compounds (Jin and Rolle, 2014; Vogt et al., 2008; Vogt et al., 2016) and micropollutants (Elsner and Imfeld, 2016; Jin and Rolle, 2016). There is also an increasing number of recent CSIA studies focusing on the photolytic transformation of organic contaminants such as organophosphorus compounds (Wu et al., 2018), chlorobenzenes (Passeport et al., 2018), methyl-tert-butyl ether (MTBE, (Zhang et al., 2015), 4-chloroaniline (Ratti et al., 2015) and atrazine (Hartenbach et al., 2008). However, to the best of our knowledge, CSIA has not yet

been used to elucidate the reaction mechanisms of TCS photodegradation. Thus, it is unclear whether carbon CSIA can be potentially used as a tool to investigate TCS photochemistry, especially to characterize different bond-cleavage reaction pathways. Moreover, the influence of different photolytic conditions on the formation and accumulation of potentially toxic transformation intermediates is not completely understood.

In this work, we assess the photodegradation mechanisms of TCS induced by simulated sunlight radiation. CSIA and Ultrahigh-Resolution Electrospray Ionization Fourier Transform Ion Cyclotron Resonance Mass Spectrometry (HR ESI FT-ICR-MS) are here used as novel instruments to evaluate the concurrent reaction pathways of TCS photodegradation. Specifically, we: i) investigate the kinetics of TCS photochemical degradation; ii) evaluate the stable carbon isotope fractionation associated with the photodegradation of TCS; iii) identify reaction by-products by means of FT-ICR-MS, and iv) develop a detailed reaction mechanism based on the detected compounds.

The present mechanistic work focuses on the direct photolysis, while indirect phototransformation will be examined in future works. TCS undergoes an acid-base equilibrium (HTric $\leftrightarrows$ H$^+$ + Tric$^-$) with pKa ~ 8.1 (Singer et al., 2003), and it has been proven that the direct photolysis of TCS is particularly important for its basic form (Tric$^-$) and much less for the undissociated one (HTric) (Bianco et al., 2015). Therefore, experiments were here focused on the direct photolysis behavior of Tric$^-$ and were carried out in the pH interval 8.4-10.5, where the basic form prevails. However, because Tric$^-$ is much more photoactive than HTric, it contributes significantly to TCS photodegradation well below pH 8 (Bianco et al., 2015). Moreover, photoreactivity parameters are known for

both HTric and Tric⁻, which allows for photochemical modelling (Bianco et al., 2015). For these reasons, and to get insight into the environmental significance of the experimental findings, modelling was carried out in this work over a pH range that extended well beyond the conditions tested in the laboratory.

2. Materials and methods

2.1. Chemicals:

Triclosan (5-chloro-2-(2,4-dichlorophenoxy)phenol, purity > 99.8%) and hexamethylbenzene (purity > 99.8%) were obtained from Dr. Ehrenstorfer (Germany). Humic acids were purchased from Sigma-Aldrich (Germany). Ethyl acetate (purity > 99.8%), isooctane (purity > 99.8%) and methanol were supplied by Aladdin (Shanghai, China), Macklin (Shanghai, China) and Merck (Darmstadt, Germany), respectively. Solvents were all of HPLC grade (Merck & Co., Germany). Hydrochloric acid was of AR grade. The used buffer solution was made with $NaHCO_3$ (purity > 99.0%) and Na_2CO_3 (purity > 99.5%), both purchased from CNW (Shanghai, China). All aqueous solutions were prepared using ultrapure water (18.2 MΩ cm⁻¹, Sartorius, Germany).

2.2. Experimental setup:

A double-wall photoreactor with a volume of 130 cm³, made out of borosilicate glass as described in details (Mekic et al., 2018a), was used to assess the photochemical degradation of TCS. Briefly, the freshly prepared solution of $3.5 \cdot 10^{-5}$ mol L⁻¹ TCS in ultra-pure water

(18.2 MΩ cm^{-1}, Sartorius, Germany), containing 5 mg L^{-1} HA when relevant, was magnetically stirred during 12 h irradiation under equilibrium with air, but without O$_2$ addition. The temperature during all the experiments was held constant at 293 K by the use of a thermostatic bath (LAUDA ECO RE 630 GECO, Germany).

A solar simulator (500 W high-pressure xenon lamp) was used to irradiate the prepared solution at two different pH values, pH 8.4 and pH 10.5, which were measured by pH/RDO/DO meter (ORION STAR A326, Thermo Scientific, USA). The infrared radiation, which might cause heating of the solution, was removed with a water filter, and a cutoff filter (300 nm ≤ λ ≤ 700 nm) was mounted on the exit beam to provide UV-Vis radiation, relevant to the lower atmosphere at the Earth's surface. A calibrated spectroradiometer (Ocean Optics, USA) equipped with a linear-array CCD detector was used to measure the spectral irradiance of the solar simulator. The comparison between the spectral irradiance emitted by the solar simulator and the solar spectral irradiance obtained with the Tropospheric Ultraviolet and Visible (TUV) model (Madronich, 1987) is shown in **Fig. S1** in the Supplementary Material, hereinafter SM.

Twenty-mL aliquots were withdrawn from the reactor at scheduled irradiation times for further analysis. The measurement of UV-Vis spectra was performed immediately after sampling. The spectra of initial (0 h) and irradiated samples (12 h irradiation time) were recorded with a UV-Vis double-beam spectrophotometer (Shanghai Drawell Scientific, China) in quartz cuvettes with 1 cm optical path length (Mekic et al., 2019). All the photochemical experiments were carried out in duplicate.

2.3. Analytical approaches:

2.3.1. Sample preparation

Liquid-liquid extraction was performed on the water samples. Briefly, a 1 mL water aliquot was adjusted to pH 4 with concentrated hydrochloric acid to obtain TCS in its protonated form (Wu et al., 2019). Separate 3×3 mL aliquots of ethyl acetate were added, coupled with centrifugation (2000 rpm) for 10 min between each addition. The supernatant ethyl acetate fractions were then combined in a separate amber glass tube, evaporated to near dryness by nitrogen blowdown, and reconstituted in 1 mL iso-octane before being transferred to a sample vial. Five hundred nanograms of hexamethylbenzene (HMB) were added as internal standard prior to instrumental analysis.

2.3.2. Concentration analysis

TCS analysis was performed using a gas chromatograph-mass spectrometer (GCMS-QP2010; Shimadzu, Kyoto, Japan), with a DB5-MS capillary column (30 m × 0.25 mm × 0.25 µm; Agilent, Santa Clara, USA) in selected ion monitoring (SIM) mode. The mass spectrometer was operated in electron impact ionization (EI) mode with the ionization potential at 70 eV. The injected sample volume was 1 µL in splitless mode. The carrier gas was helium with a constant flow rate of 1.2 mL min^{-1}. The temperature of inlet and ion source was maintained at 280°C and 230°C, respectively. The GC oven temperature started at 80°C for 2 min and then increased to 280°C at a rate of 20°C min^{-1}, holding for 5 min. The selected quantitative and qualitative ion fragments were m/z 218 and 288 for TCS, and m/z 147 and 162 for HMB (see **Fig. S3** in SM). The internal standard method was applied for

quantitative analysis. The linear regression coefficient of the calibration curve was at least 0.9991.

2.3.3. Compound-specific carbon isotope analysis

Stable carbon isotope analysis was performed by gas chromatography, using a Trace GC Ultra connected through a GC-IsoLink to a Delta V Advantage isotope ratio mass spectrometer (Thermo Fisher Scientific, USA). The inlet temperature was 290°C. The samples were preconcentrated by about 20 times, and were then injected in splitless mode and separated by the same column as used in GCMS-QP2010. The GC oven temperature was also programmed in the same way as before.

2.3.4. Analysis of the photodegradation products using FT-ICR-MS

The fresh sample aliquots of photodegraded TCS were diluted 1:9 (by volume) with methanol, and further analyzed with a solariX XR FT-ICR-MS (Bruker Daltonik GmbH, Bremen, Germany) instrument. This instrument is equipped with a refrigerated, 9.4 T actively shielded superconducting magnet (Bruker Biospin, Wissembourg, France) and a Paracell analyzer cell. The obtained samples were ionized in the negative ion mode by ESI ion source (Bruker Daltonik GmbH, Bremen, Germany). The mass range of detection was set to m/z 150–1000, while ion accumulation time was set to 0.65 s (Mekic et al., 2018b). A total of 64 continuous 4M data FT-ICR transients were co-added to enhance the signal-to-noise ratio and dynamic range (Jiang et al., 2014; Shi et al., 2012). Using a linear calibration, all the mass spectra were calibrated externally in the negative ion mode by use of arginine

clusters (Shi et al., 2012). The final spectrum was internally recalibrated with typical O_2 class species peaks, using quadratic calibration in DataAnalysis 4.4 (Bruker Daltonics) (Jiang et al., 2014; Shi et al., 2012). A typical mass-resolving power (m/Δm 50%, in which Δm50% is the magnitude of the mass spectral peak full width at half-maximum peak height) > 450,000 was achieved at *m/z* 319, with < 0.3 ppm absolute mass error. The data were processed by a well-described methodology (Jiang et al., 2014; Shi et al., 2012).

2.4. Modeling Approaches

2.4.1. Kinetic data treatment

The time trend of TCS under irradiation followed pseudo-first order kinetics decay down to a plateau. The reason for this behavior may be the inhibition of photodegradation by the transformation intermediates, which could either compete with the parent compound for radiation absorption, or undergo back-transformation into the original compound. The resulting time trend can be fitted with a first-order kinetic equation with residual, of the form $C_t/C_o = 1 + A \ (e^{-kt} - 1)$, where C_t is the concentration of TCS at the time *t*, C_o its initial concentration, *k* the pseudo-first order transformation rate constant, while *A* defines the residual concentration C_r ($C_r = C_o \ (1 - A)$). The initial rate of TCS degradation can be calculated as $R_o = (dC_t/dt)_{t=0} = k \ A \ C_o$.

2.4.2. Photochemical modeling

The phototransformation kinetics of TCS was modeled with the APEX software (Aqueous Photochemistry of Environmentally-occurring Xenobiotics), by assuming fair-weather, mid-

latitude sunlight irradiation during the summer season, and depth and chemistry of water as suitable for surface-water environments. In this study, 0.1 mmol L^{-1} nitrate, 1 µmol L^{-1} nitrite, 1 mmol L^{-1} alkalinity, dissolved organic carbon, DOC, in the range of 1 to 10 mg$_C$ L^{-1}, and 5 m water depth were defined and input in the model (Bodrato and Vione, 2014). In addition to predicting the overall phototransformation kinetics, APEX is also able to assess the importance of the different photochemical pathways as a function of variable environmental conditions. The respective reaction rate constants of HTric (acidic TCS form) and Tric$^-$ (basic TCS form) with $^\bullet$OH (respectively, 5.4×10^9 and 1×10^{10} L mol^{-1} s^{-1}), CO$_3^{\bullet-}$ (4.2×10^7 L mol^{-1} s^{-1} for Tric$^-$, $k_{HTric+CO_3^{\bullet-}}$ unknown but probably negligible), ^{1}O$_2$ (3×10^6 and 1.1×10^8 L mol^{-1} s^{-1} for HTric and Tric$^-$, respectively) and ^{3}CDOM* (3.1×10^9 and 4.3×10^9 L mol^{-1} s^{-1} for HTric and Tric$^-$, respectively), as well as the direct photolysis quantum yield (0.4, as a reasonable average value of the available data, without evidence of a pH trend) were used as APEX input data and taken from the literature (Bianco et al., 2015; Buth, 2009; Huang et al., 2018; Latch et al., 2005). Radiation absorption (absorbed photon flux P_a^x) by x = HTric/Tric$^-$ and the main photosensitisers (x = CDOM, NO$_3^-$ and NO$_2^-$) was computed by APEX taking into account competition for irradiance in a sunlight-absorbing mixture, according to a Lambert-Beer approach (Bodrato and Vione, 2014):

$$P_a^{CDOM} = \int_\lambda p°(\lambda)(1-10^{-A_{CDOM}(\lambda)})d\lambda \tag{1}$$

$$P_a^y = \int_\lambda p°(\lambda)\frac{A_y(\lambda)}{A_{CDOM}(\lambda)}(1-10^{-A_{CDOM}(\lambda)})d\lambda \tag{2}$$

where y = HTric, Tric⁻, NO_3^- or NO_2^-, $A_{CDOM}(\lambda)$ is the absorbance of CDOM and $A_y(\lambda)$ the absorbance of the other relevant light-absorbing species.

The modeled first-order photodegradation rate constants k_{HTric} and k_{Tric^-} are computed separately for the HTric and Tric⁻ species, respectively, but it is also possible to determine the overall transformation rate constant of TCS, $k_{TCS} = k_{HTric}\,\alpha_{HTric} + k_{Tric^-}\,\alpha_{Tric^-}$. Here, $\alpha_{HTric} = [H^+]\cdot([H^+]+K_a)^{-1}$ and $\alpha_{Tric^-} = K_a\cdot([H^+]+K_a)^{-1}$ are the respective molar fractions of HTric and Tric⁻, and $K_a \sim 10^{-8.1}$ (Singer et al., 2003). More information about photochemical modeling is available in the Supplementary Material (hereinafter SM).

2.4.3. Evaluation of stable carbon isotope ratios

The bulk stable carbon isotope ratios (R) are expressed by the ratio between ¹³C and ¹²C abundances. In order to correlate concentration of the target compound with stable isotopic ratios, the Rayleigh approach is applied. The enrichment factor ε_{bulk} can be obtained from the slope of the Rayleigh correlation (Rayleigh, 1896):

$$\ln\frac{R_t}{R_0} = \varepsilon_{bulk}\,\ln\frac{C_t}{C_0} \qquad (3)$$

where R_t and R_0 represent isotope ratios at a specific time t and initial average isotopes ratio of contaminant, respectively. For instance, the enrichment factor of carbon isotopes can represent the extent of carbon isotope fractionation of a certain compound that occurs during degradation processes. Therefore, the enrichment factors can be experimentally determined. To further derive kinetic isotope effects at reactive positions, it is necessary to recover the

"dilution effects" by isotopes at non-reactive positions. The apparent kinetic isotope effect (AKIE) for a specific reaction pathway is calculated according to the following equation (Elsner et al., 2005):

$$AKIE = \frac{1}{1 + \varepsilon_{reactive\ position}} \approx \frac{1}{1 + n / x \cdot \varepsilon_{bulk}} \qquad (4)$$

where ε_{bulk} is the bulk carbon enrichment factor, n is the number of total carbon atoms in the molecule, and x is the number of carbon atoms located at reactive positions.

2.4.4. In-silico toxicity assessment

ECOSAR V2.0 software [Ecological Structure Activity Relationships (ECOSAR) Class Program] (Reuschenbach et al., 2008) was used to determine acute-toxicity parameters (LC_{50} and EC_{50}) and chronic toxicity values (ChV) to aquatic organisms. The software is free of charge and available on the web page of U.S. EPA (*https://www.epa.gov/tsca-screening-tools/ecological-structure-activity-relationships-ecosar-predictive-model*) (Mayo-Bean, 2012). The molecular structures can be entered into ECOSAR by means of a graphical interface, and the software derives toxicity by means of a structure-activity approach that takes into account the functional groups as well as the calculated physico-chemical properties of the compound. The tested molecules were both TCS and its identified transformation intermediates. The detailed information of this software is available in the SM.

3. Results and Discussion

3.1. Reaction kinetics and HA effect on TCS direct photolysis

Figure 1 shows that the addition of 5 mg L^{-1} HA inhibited the photodegradation of TCS at pH 10.5. Under these conditions, where Tric$^-$ is the prevalent TCS species (Singer et al., 2003), HA lowered the initial TCS degradation rate by about 3.3 times. A first reason for HA to inhibit the direct photolysis of Tric$^-$ is competition for lamp irradiance between the two species, i.e., Tric$^-$ and HA. Considering that the absorption spectra of Tric$^-$ and HA overlap in the wavelength region where the lamp emits radiation (**Fig. S1** in SM), it is possible to compute the extent of Tric$^-$ absorption inhibition carried out by HA. It is possible to normalize $p°(\lambda)$ as $\gamma_\lambda = p°(\lambda) (p°_{max})^{-1}$, where $p°(\lambda)$ is the spectral photon flux density of the lamp received by the solution at the wavelength λ, and $p°_{max}$ is the maximum value of $p°(\lambda)$. Then, the ratio ρ between the photon fluxes absorbed by Tric$^-$ alone in solution and in the presence of HA can be expressed as follows (Braslavsky et al., 2007):

$$\rho = \frac{\int_\lambda \gamma_\lambda \dfrac{A_{Tric^-}(\lambda)}{A_{Tric^-}(\lambda) + A_{HA}(\lambda)} \{1 - 10^{-b[A_{Tric^-}(\lambda) + A_{HA}(\lambda)]}\} d\lambda}{\int_\lambda \gamma_\lambda \{1 - 10^{-b A_{Tric^-}(\lambda)}\} d\lambda} \qquad (5)$$

where $A_{Tric^-}(\lambda)$ and $A_{HA}(\lambda)$ are the absorbance values of, respectively, Tric$^-$ and HA at the concentrations used in the irradiation experiments, measured over an optical path length $b = $ 1 cm as per the spectrophotometric measurements.
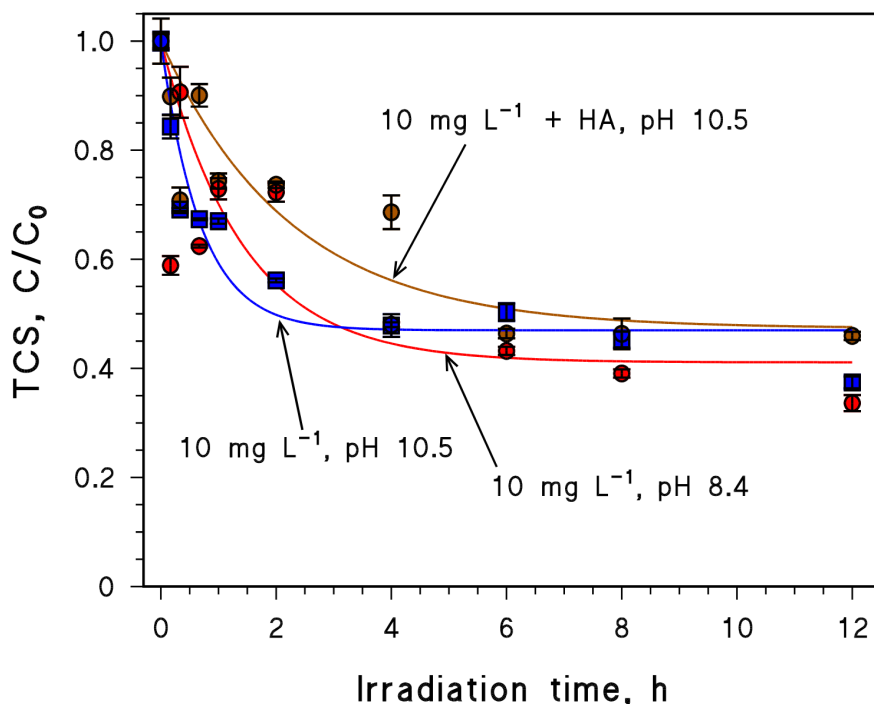
Figure 1. TCS photodegradation profiles observed in different irradiation conditions (different pH values, presence or absence of HA). The error bounds represent the standard error of replicate measurements (semi-difference of the duplicate experimental data).

In the photoreactor, the path traveled by light was considerably longer (b = 20 cm in **Eq. (5)**). The calculation yielded ρ = 0.6, which means that HA should decrease the value of R_o by approximately 40% due to irradiance competition.

The actual inhibition carried out by HA on Tric⁻ photodegradation was considerably higher than suggested by light-absorption calculations (the Tric⁻ photodegradation rate was 70% lower in the presence of HA), thus an additional inhibition pathway can be reasonably assumed. The primary step in the direct photolysis of Tric⁻ is known to be its transformation into a phenoxyl radical (Kliegman et al., 2013), which is a rather common step for phenolic compounds (Braslavsky et al., 2007; Net et al., 2009). The phenoxyl radical, Tric•, would be

destabilized by the electron-withdrawing nature of the three chlorine atoms occurring in its two aromatic rings, and it could thus be less stable than many phenoxy radicals deriving from the oxidation of electron-rich phenolic groups occurring in HA. Therefore, the HA phenolic moieties might be involved in the back-reduction of Tric$^\bullet$ to Tric$^-$. This phenomenon has already been described in the framework of the triplet-sensitized oxidation of contaminants, where natural organic matter may inhibit degradation by reducing the partially oxidized substrates back to the parent compounds (Leresche et al., 2016; Wenk and Canonica, 2012). Interestingly, similar species (e.g., phenoxy radicals) may be produced by different processes such as direct photolysis and triplet sensitization (Berto et al., 2016; Lu, 2002). In this framework, in analogy with the anti-oxidant effect of organic matter in the context of triplet sensitization (Wenk and Canonica, 2012), and considering that different processes than the direct photolysis may also be operational for Tric$^-$ in HA solution, the first-order photodegradation rate constants of Tric$^-$ alone ($k_{Tric^-}^{o}$) and in the presence of HA ($k_{Tric^-,HA}$) would be linked as follows:

$$\xi\, k_{Tric^-,HA} = \rho\, k_{Tric^-}^{o}\, \frac{1}{1+\dfrac{DOC}{DOC_{1/2}}} \qquad (6)$$

where ξ is the fraction of Tric$^-$ undergoing direct photolysis upon irradiation in the presence of HA, ρ is given by **Eq. (5)**, DOC is the value of the dissolved organic carbon accounted for by the natural organic matter (HA in the present case), and $DOC_{1/2}$ measures the anti-oxidant effect of the organic matter (the lower is $DOC_{1/2}$, the higher is the effect) (Wenk and

Canonica, 2012). To assess the value of $DOC_{1/2}$ in the present case, the following considerations should be taken into account: *(i)* HA at the used concentration have DOC = 0.75 mg_C L^{-1}; *(ii)* ρ = 0.6 takes into account the light-screening effect of HA (**Eq. (5)**); *(iii)* thanks to the results of a previous study (Bianco et al., 2015) we can expect that, in the presence of HA under our experimental conditions (DOC = 0.75 mg_C L^{-1}), the photochemical transformation of $Tric^-$ proceeds by 90% upon direct photolysis and by the remaining 10% upon triplet sensitization (reaction with HA triplet states, $^3HA^*$), $^{\bullet}OH$ and $^1O_2$ reaction (Bianco et al., 2015), thereby yielding ξ = 0.9; *(iv)* experimentally, one has $k_{Tric^-,HA} = 0.3 \; k^o_{Tric^-}$. On this basis, one gets $DOC_{1/2}$ = 0.6±0.3 mg_C L^{-1}. Interestingly, this is very near the value estimated for the anionic form of sulfadiazine in the framework of triplet sensitization (Vione et al., 2018).
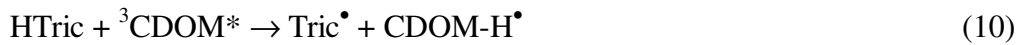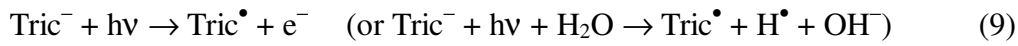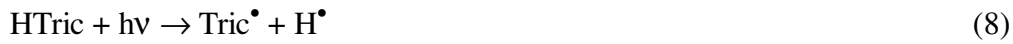
3.2. Insights from photochemical modeling

The APEX modeling of TCS photodegradation should take into account the antioxidant effect of organic matter on the direct photolysis as assessed in this work (note that APEX already considers by default the competition for irradiance between CDOM and xenobiotics). The most straightforward way to include the anti-oxidant effect into the simulations is to assume that it lowers by a factor $\psi < 1$ the direct photolysis quantum yield of TCS:

$$\Phi_{TCS} = \Phi^o_{TCS} \; \psi = \Phi^o_{TCS} \frac{1}{1 + \dfrac{DOC}{DOC_{1/2}}} \qquad (7)$$

where $\Phi^o_{TCS} = 0.4$ is the direct photolysis quantum yield of TCS without other sources of organic matter (Latch et al., 2005; Buth et al., 2009), and Φ_{TCS} is the quantum yield at the given DOC value.

From a mechanistic point of view, the anti-oxidant effect is likely caused by Tric$^\bullet$ reduction. However, the same phenoxy radical Tric$^\bullet$ is also the intermediate of HTric direct photolysis and of TCS (*i.e.*, both HTric and Tric$^-$) oxidation by ^{3}CDOM* (Bianco et al., 2015). A similar effect is thus expected on the triplet-sensitized transformation process. Note that **reaction (9)** describes the overall stoichiometry of Tric$^-$ direct photolysis, but it is not necessarily suggesting mechanistic details with production of solvated e$^-$ (*vide infra*).

$$\text{HTric} + h\nu \rightarrow \text{Tric}^\bullet + \text{H}^\bullet \tag{8}$$

$$\text{Tric}^- + h\nu \rightarrow \text{Tric}^\bullet + e^- \quad (\text{or Tric}^- + h\nu + \text{H}_2\text{O} \rightarrow \text{Tric}^\bullet + \text{H}^\bullet + \text{OH}^-) \tag{9}$$

$$\text{HTric} + {}^3\text{CDOM}* \rightarrow \text{Tric}^\bullet + \text{CDOM-H}^\bullet \tag{10}$$

$$\text{Tric}^- + {}^3\text{CDOM}* \rightarrow \text{Tric}^\bullet + \text{CDOM}^{\bullet-} \tag{11}$$

Therefore, in analogy with the direct photolysis, we assume that the factor $\psi = (1 + \text{DOC}/\text{DOC}_{1/2})^{-1}$ that describes the antioxidant effect on phototransformation also applies to the case of the reaction rates of HTric and Tric$^-$ with ^{3}CDOM*. Based on this consideration and on the second-order **reactions (10,11)**, we can write the relevant rates as follows:

$$R_{HTric+^3CDOM*} = \psi \, R^o_{HTric+^3CDOM*} = \psi \, (k^o_{HTric, ^3CDOM*} [HTric][^3CDOM*]) \tag{12}$$

$$R_{Tric^- + {}^3CDOM*} = \psi\, R^o_{Tric^- + {}^3CDOM*} = \psi\,(k^o_{Tric^-, {}^3CDOM*}[Tric^-][{}^3CDOM*]) \tag{13}$$

The most straightforward way to include this anti-oxidant effect within the APEX software is to assume $k_{HTric, {}^3CDOM*} = \psi\, k^o_{HTric, {}^3CDOM*}$ and $k_{Tric^-, {}^3CDOM*} = \psi\, k^o_{Tric^-, {}^3CDOM*}$, which is equivalent to assuming that the anti-oxidant effect lowers the second-order reaction rate constants between HTric/Tric⁻ and ³CDOM* (Vione et al., 2018). Therefore, the degradation rates were expressed as follows:

$$R_{HTric + {}^3CDOM*} = k_{HTric, {}^3CDOM*}[HTric][{}^3CDOM*] \tag{14}$$

$$R_{Tric^- + {}^3CDOM*} = k_{Tric^-, {}^3CDOM*}[Tric^-][{}^3CDOM*] \tag{15}$$

Figure 2 reports the simulation results, highlighting the roles of the different photoprocesses (**2a**) and of the two species (HTric and Tric⁻, **2b**) in TCS photodegradation as a function of pH, as well as the effect of the DOC on Tric⁻ phototransformation (**2c**). It is apparent that TCS becomes increasingly photolabile as the pH increases (**Figure 2a**), due to the higher photolability of Tric⁻ compared to HTric. This finding is in agreement with previous results that did not consider the back-reduction effect (Bianco et al., 2015). Tric⁻ is noticeably very photolabile, with typical summer lifetimes ranging from one day at low DOC to a couple of weeks at high DOC (**Figure 2c**). Tric⁻ photodegradation is inhibited by the presence of natural organic compounds that are quantified as the water DOC, coherently with our experimental findings according to which TCS phototransformation at pH 10.5 was inhibited by HA (**Figure 1**).
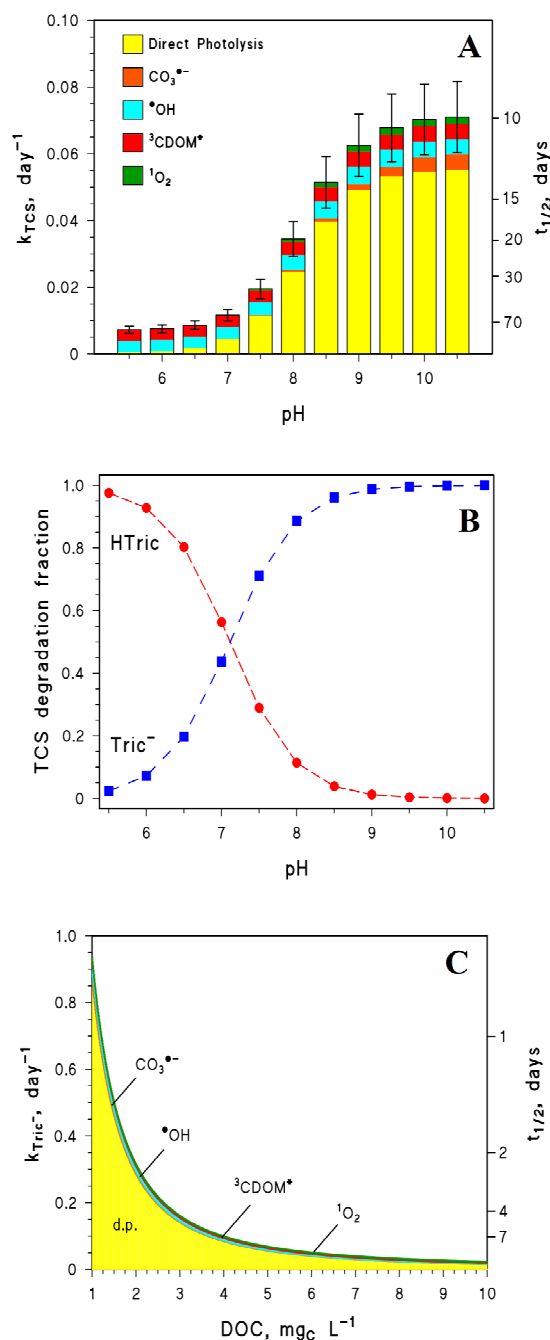
Figure 2. **(A)** Simulated pseudo-first order photodegradation rate constants of TCS (left Y-axis) and corresponding half-life times (fair-weather sunny days, right Y-axis), as a function of pH (DOC = 5 mg$_C$ L^{-1}). The role of the different photochemical processes is highlighted with different colors. **(B)** Trend with pH of the relative roles of HTric and Tric$^-$ in TCS photodegradation (DOC = 5 mg$_C$ L^{-1}). **(C)** Tric$^-$ photodegradation kinetics as a function of the water DOC (d.p. = direct photolysis). Other conditions: 10^{-4} mol L^{-1} nitrate, 10^{-6} mol L^{-1} nitrite, 10^{-3} mol L^{-1} alkalinity, 5 m water depth. The error bounds in **(A)** are the sigma-level model uncertainties on the values of the overall pseudo-first order degradation rate constants of TCS.

Reactions with $^{\bullet}OH$ and $^3CDOM^*$ are predicted to play the main roles in the photodegradation of HTric, while the direct photolysis would predominate in the case of Tric$^-$. Moreover, because Tric$^-$ is photodegraded faster than HTric, it would play the main role in TCS photodegradation at pH > 7-7.5 (**Figure 2b**). These pH conditions are very relevant to surface-water environments and, because the direct photolysis of Tric$^-$ is also known to produce toxic by-products (Bianco et al., 2015), we now focus our attention on the photodegradation of Tric$^-$ by direct photolysis. Further experiments are thus carried out at pH 8.4 and especially 10.5, where Tric$^-$ strongly prevails. At pH 10.5, one is confident that only the behavior of the basic form is studied.

3.3. Molecular composition by ultra-high resolution mass spectrometry

The analysis performed by FT-ICR-MS revealed that the molecular composition of the products formed upon 12 hours of TCS irradiation was very complex (see **Fig. S5** in the SM). The iso-abundance plot of DBE (double-bond equivalent, namely the number of double bonds plus rings present in the organic compounds) versus carbon numbers for the detected $C_aH_bO_cCl_d$ species in this work is presented in **Fig. S6**.

The commonly used way for the visualization and interpretation of high resolution-mass spectrometry (HR-MS) data is the van Krevelen diagram, which presents the H/C ratio as a function of O/C. This diagram is a useful tool to outline the compositional characteristics of the identified high-molecular weight compounds, which differ in chemical mass building increments. However, in the typical van Krevelen diagram (H/C vs. O/C) (Mekic et al., 2018b) the relevant classes of compounds, based on ions like $C_aH_bO_cCl_d^-$, are located very

close together and it is complicated to distinguish the mass increments. Therefore, in order to focus on the Cl component of the $C_aH_bO_cCl_d$ compounds, we used a modified version of the van Krevelen diagram, obtained by plotting the Cl/C ratio versus O/C (**Figure 3**).
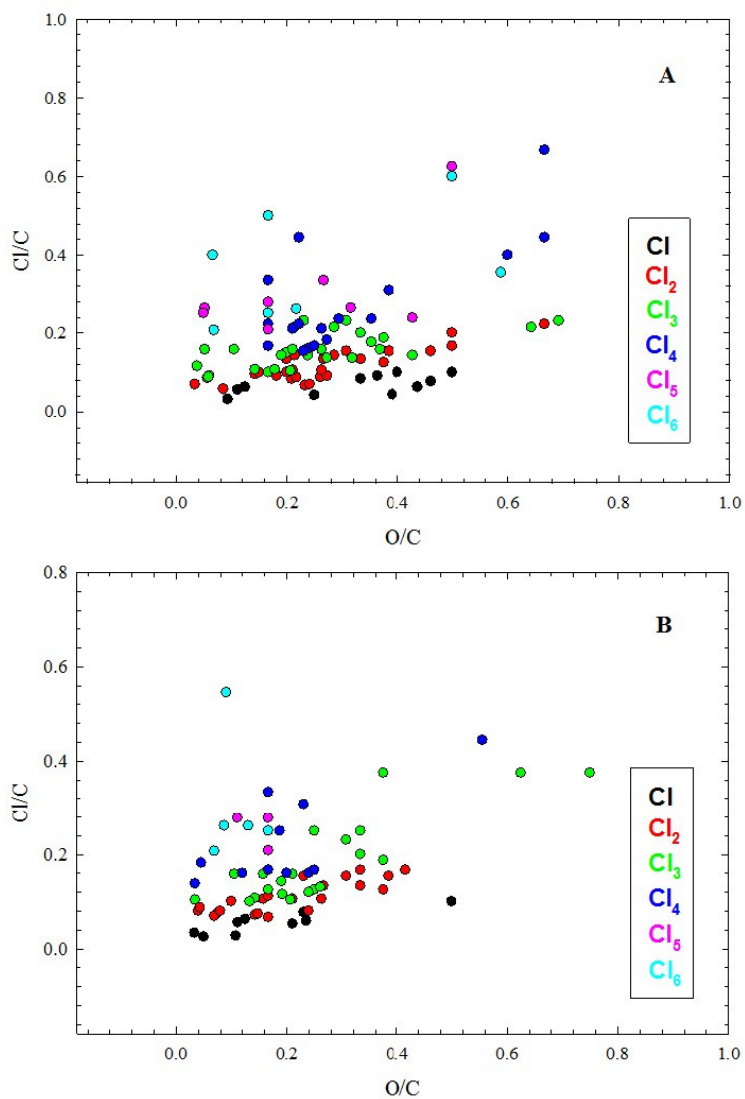
Figure 3. van Krevelen diagram, illustrating the compounds class of $C_aH_bO_cCl_d$ produced upon photodegradation of TCS in two different conditions; A) pH 10.5 and B) pH 8.4. The FT-ICR-MS data are scanned in negative mode.

In this Cl-based van Krevelen diagram, certain mechanistic patterns become evident and the

$C_aH_bO_cCl_d$ compounds can be identified. There is a series of compounds that contain an unchanged number of Cl atoms and differ by different mass units (**Table S1**). For example, with the addition of CH_2O_3, the DBE value remains unchanged indicating that the number of rings and double bonds does not change in the molecule and that, therefore, the addition of this block increment occurs only through single bonds (Altieri et al., 2009). The same applies for the addition of other identified block increments including C_3H_6O, C_2H_4O, and CH_2O (**Table S1**). These patterns suggest that some of the detected $C_aH_bO_cCl_d$ compounds could be formed through oligomerization reactions (**Scheme 1**, vide infra) initiated by the light-induced degradation of TCS.

3.4. Reaction mechanism based on the detected by-products

Based on the compounds detected by FT-ICR-MS analysis, the detailed reaction pathways were developed and they are depicted in **Scheme 1**. We suggest that TCS undergoes initial phototransformation into four main by-products, namely 2,4-dichlorophenol, 4-chlorocatechol, 3-chlorophenol and 1,3-dichlorobenzene.

Hydrogen-bond complexes between TCS and other molecules could account for several recorded *m/z* signals. In particular, the *m/z* signal 574.9 is likely accounted for by a TCS+TCS complex, *m/z* 430.9 by TCS+4-chlorocatechol, and *m/z* 448.9 by TCS+2,4-dichlorophenol. The *m/z* 540.9 compound might also derive from hydrogen-bond complexation, as it could be generated by the interaction between *m/z* 412.9 (see later its formation) and 3-chlorophenol.
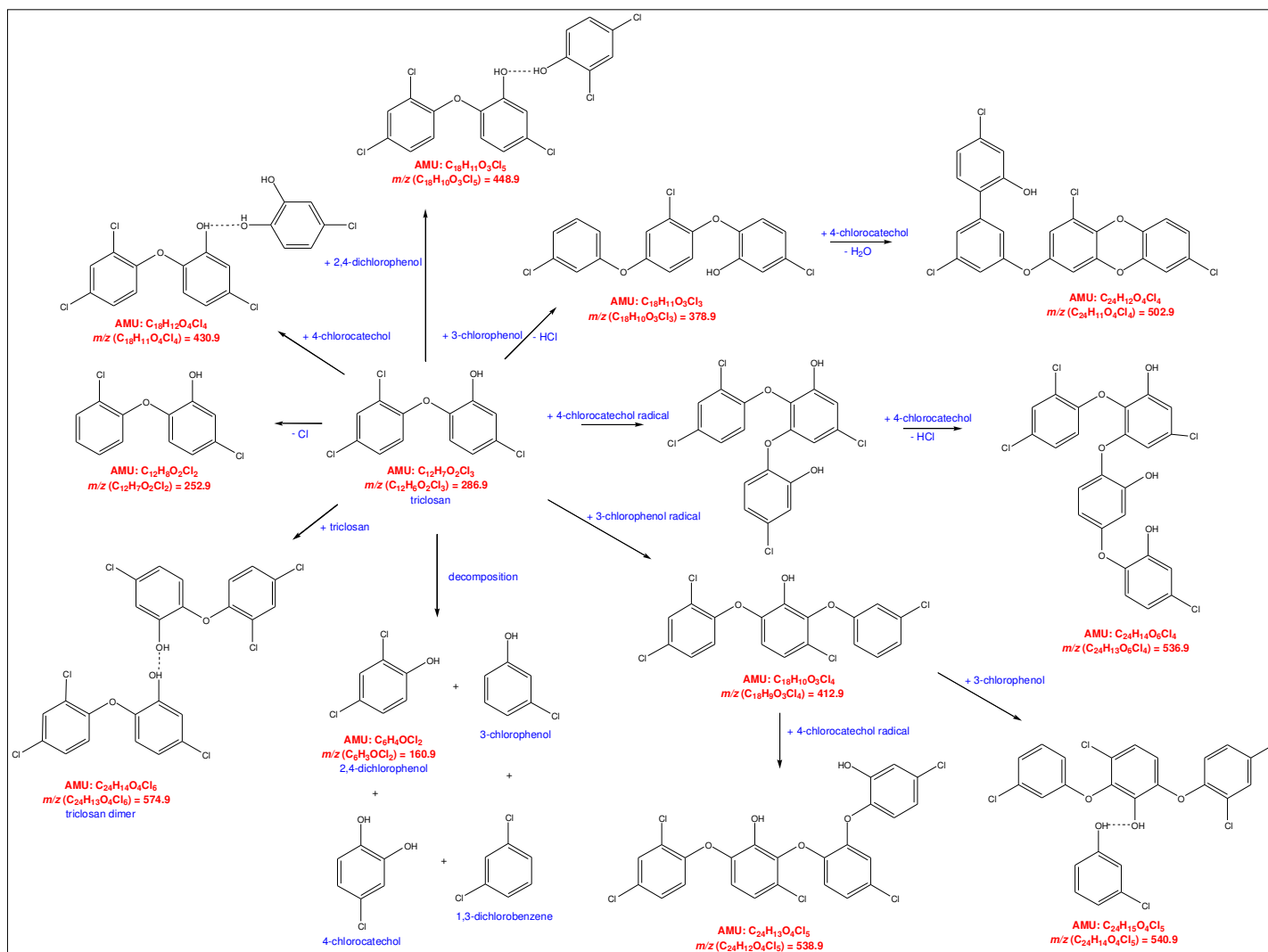
Scheme 1. Proposed reaction mechanism for light-induced degradation of TCS at pH 10.5. The short dashed lines represent hydrogen bonds between molecules.

The formation of such hydrogen bonded complexes is commonly observed in ESI mass spectra (Pan, 2008). Concerning actual molecules, TCS might form a product with 3-chlorophenol (m/z 378.9) by releasing one HCl molecule. With subsequent addition of 4-chlorocatechol, m/z 536.9 could be produced by dehydration (- H_2O).

The formation of the high-molecular weight product m/z 538.9 could be ascribed to radical-initiated reactions between 3-chlorophenoxyl radical and TCS, forming a species with m/z 412.9, followed by addition of 4-chlorocathecol and HCl loss. Similarly, the reaction between TCS and two 4-chlorocatecholyl radicals followed by HCl release could account for the m/z 536.9 signal. The HCl loss is in agreement with stable carbon isotope fractionation analysis, which suggests that C-Cl cleavage is favorable (see the next section).

The occurrence of TCS oligomerization processes leading to the formation of high-molecular weight compounds is consistent with the time evolution of the TCS UV-Vis absorption spectra, which evolve from molecular bands into an exponential-like continuum (see **Fig. S3**). Such a behavior has already been reported (Vione et al., 2019) and seems to be typical of oligomerization processes (De Laurentiis et al., 2013b).

The potential toxicity of the transformation intermediates was tentatively assessed by a quantitative structure-activity relationship approach (ECOSAR software; more detailed information and full data are available in **Table S3** and associated text). The parent TCS is predicted to be more toxic toward fish and crustaceans than to algae, while the monoaromatic transformation intermediates should be consistently less

toxic than TCS. In contrast, a significant toxicity increase is predicted for the intermediates having three to four aromatic rings that, like TCS, should be more toxic to fish and crustaceans than to algae.

Among the transformation intermediates, the occurrence of dioxin-like compounds is also concerning. For example, the formation of 2,8-dichlorodibenzo-*p*-dioxin was identified by the use of GC-MS (see SM), which is in good agreement with previous studies (Chen et al., 2008; Constantin et al., 2018; Latch et al., 2005; Lores et al., 2005). The identified dioxin is likely to be less toxic to aquatic organisms than the intermediates with 3 or 4 aromatic rings, but toxicity to mammals could be an issue, and even to fish if the detoxification metabolism is blocked (Sijm and Opperhuizen, 1988).

3.5. Bond-cleavage reaction pathways and stable carbon isotope fractionation

Influence of pH: As discussed above, the initial photolysis rate of TSC was higher at pH 10.5 (7.4×10^{-9} mol L^{-1} s^{-1}) than at pH 8.4 (4.0×10^{-9} mol L^{-1} s^{-1}). At the higher pH value, TCS is fully deprotonated as Tric$^-$ in aqueous solution. In addition to enhancing photodegradation, higher pH also resulted in a higher enrichment factor ε_{bulk} (see **Eq. (3)**), -3.48‰, in comparison with the experiment at pH 8.4 (-1.74‰). The apparent kinetic isotope effects (AKIEs, see **Eq. (4)**) were derived, too, and they are summarized in **Table 2**. The AKIEs were 1.044 and 1.022 for pH 10.5 and pH 8.4, respectively. AKIE at pH 8.4 was very close to the theoretical carbon kinetic isotope effect (1.021) calculated for C-H bond cleavage following Streitwieser Semiclassical theory (Cooket al. 1991) (see **Table S2** in SM), whereas the AKIE obtained at pH

10.5 was lower than the theoretical values for the bond cleavage of C-Cl (1.057) and C-O (1.061). These results suggest that different fractions of bond-cleavage reaction pathways occurred at different pH values. Specifically, at pH 8.4 the oligomerization of TCS initiated by C-H bond breaking is predicted to be the predominant pathway. At pH 10.4, a much higher carbon AKIE value (1.044) suggests that the pathways associated with C-Cl and C-O bond cleavage are more favorable, therefore forming chlorinated phenols and other less chlorinated compounds as main reaction by-products (see **Scheme 1**).

Different initial TCS concentration: Significant carbon isotope fractionation occurred at different initial TCS concentrations, including 5 mgL^{-1}, 10 mgL^{-1}, and 30 mgL^{-1}. Different enrichment factors (ε), ranging from -4.48‰ to -2.59‰, were obtained in the Rayleigh plot (see **Fig. 4**).

As shown in **Table 1**, the AKIE values were much higher at the lower TCS concentrations (C_0). In these conditions, the reaction pathways associated with C-Cl as well as C-O bonds breaking should prevail. These pathways can account for the formation of monoaromatic chlorinated species, sometimes with fewer chlorine atoms compared to the original TCS (see **Scheme 1**). However, a much smaller AKIE value was obtained at 30 mgL^{-1}, and this value is close to the theoretical value for C-H bond breaking (1.021).
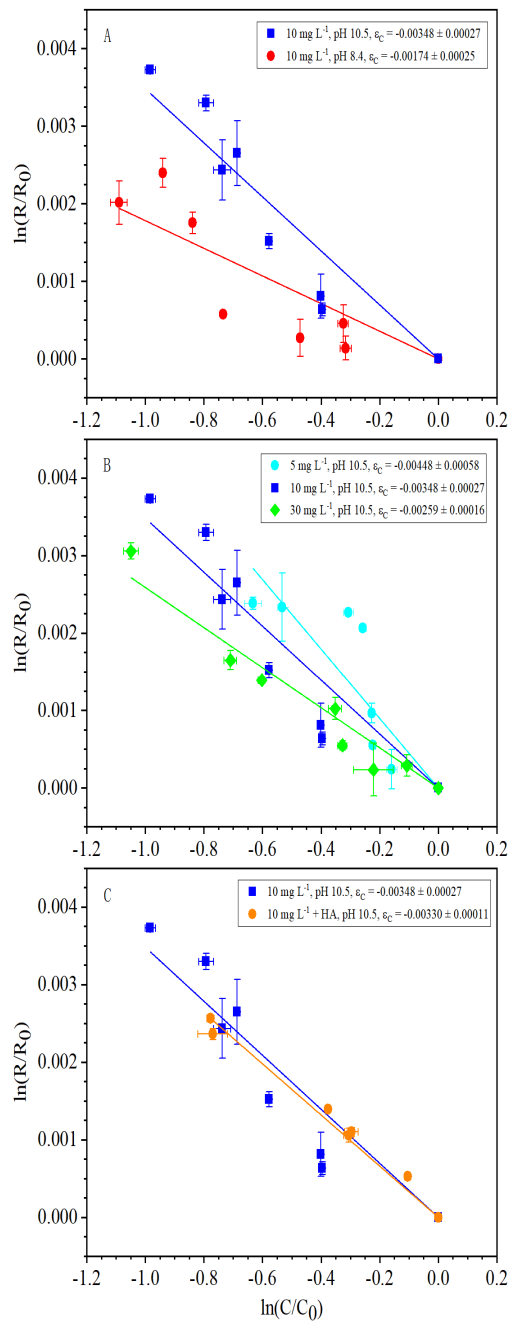
Figure 4. Stable carbon isotope fractionation during TCS photodegradation under simulated sunlight. Effect of different pH values **(a)**, initial TCS concentrations **(b)** and humic acid addition **(c)** on the stable carbon isotope ratios of TCS. Error bars represent the 95% confidence intervals. The time trend of carbon isotope ratios is available in the SM.

Influence of HA: Although HA inhibited TCS photodegradation, which is in agreement with previous literature reports (Tixier et al., 2002), it is unclear whether or not it can also affect the reaction mechanism. As shown in **Fig. 4**, a smaller extent of TCS carbon isotope fractionation was observed in the presence of HA. This might be due to the HA-induced inhibition effects. However, very similar AKIE values were obtained with and without HA (see **Table 1**), thereby suggesting that HA is unlikely to affect much the concurrent photoreaction pathways other than by slowing their kinetics down. Indeed, TCS direct photolysis is expected to strongly prevail over photosensitized processes that could be triggered by HA at pH 10.5 (see **Figure 2a**).

Table 1. Enrichment factor (ε_c) and AKIE$_C$ values in the photodegradation of TCS.

Experiment	C_0(mg L^{-1})	pH	ε_c(‰)	AKIE$_C$
1	10	8.4	-1.74 ± 0.25	1.022 ± 0.003
2	10	10.5	-3.48 ± 0.27	1.044 ± 0.004
3	30	10.5	-2.59 ± 0.16	1.032 ± 0.002
4	5	10.5	-4.48 ± 0.58	1.057 ± 0.008
5	10 (+ HA)	10.5	-3.30 ± 0.11	1.041 ± 0.001

It is interesting to observe that the TCS oligomerization pathways are likely to involve phenoxy radicals, as is typical of phenolic compounds (De Laurentiis et al., 2013b). However, they seem also to be related to C-H bond breaking, as observed in the experiments with 30 mgL^{-1} TCS, where the formation of oligomers was most enhanced. The photolysis of undissociated (neutral) phenols under UVA irradiation

has been shown by laser flash photolysis experiments to proceed through the homolytic breaking of the phenolic O-H bond, to produce the corresponding phenoxy radicals (De Laurentiis et al., 2013a). The release of a hydrogen atom (H$^\bullet$) upon irradiation cannot be detected by laser flash photolysis (differently from solvated electrons), due to poor radiation absorption by H$^\bullet$.

As far as the basic forms of phenols (phenolates, aka phenoxides) are concerned, there is evidence that UVC irradiation causes photoionization. Indeed, the generated solvated electrons have been detected with the laser flash photolysis technique. In this case, photoionization yields phenoxy radicals from phenolates (Zhao et al., 2010). In contrast, there is evidence against the formation of aquated electrons in the case of the UVA irradiation of nitrophenolates (Barsotti et al., 2017). It is quite puzzling to account for the formation of phenoxy radicals from phenolates without invoking photoionization, but the present results obtained with Tric$^-$ suggest an interesting way out of the problem. If a C-H bond is broken with production of H$^\bullet$ that escapes detection, and is thus in agreement with the available laser flash photolysis data, the lone electron on the aromatic moiety could migrate to the phenoxide oxygen where it is stabilized. The resulting negative charge on the ring C atom could be compensated for by protonation in aqueous solution. The proposed reaction pathway is depicted in **Scheme 2**, and it accounts for the formation of a phenoxy radical via C-H bond breaking.
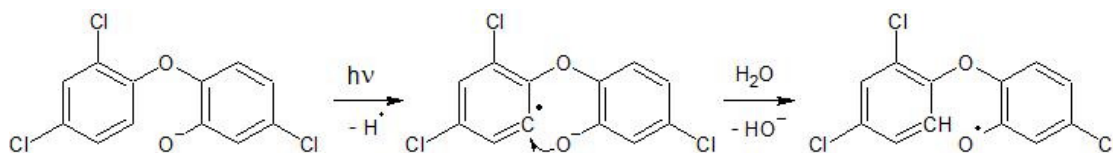
Scheme 2 Proposed photoreaction pathway for the formation of a phenoxy radical from Tric⁻, triggered by an initial C-H bond breaking.

4. Conclusions

We obtained molecular-level insights into the photochemical degradation of TCS in different conditions. The TCS photodegradation kinetics was influenced by parameters such as initial concentration, pH and presence of humic acid. In particular, humic acid inhibited TCS photodegradation because of light-absorption competition and (probably) also back-reduction effects. Moreover, photochemical modeling showed that direct photolysis should be the main Tric⁻ photodegradation pathway in surface waters, which is in good agreement with the present experimental findings. In addition, significant stable carbon isotope fractionation was observed in all the experiments, indicating cleavage of different chemical bonds by direct photolysis. The AKIEs values, determined for each experiment, suggest that pH and initial TCS concentration might affect the reaction mechanisms and form specific products. A broad and complex spectrum of organic products, some of them potentially toxic, were identified by FT-ICR-MS.

Acknowledgements

References

Aiken, G.R., Hsu-Kim, H., Ryan, J.N., 2011. Influence of dissolved organic matter on the environmental fate of metals, nanoparticles, and colloids. Environ Sci Technol 45, 3196-3201.

al Housari, F., Vione, D., Chiron, S., Barbati, S., 2010. Reactive photoinduced species in estuarine waters. Characterization of hydroxyl radical, singlet oxygen and dissolved organic matter triplet state in natural oxidation processes. Photochem Photobiol Sci 9, 78-86.

Altieri, K., J Turpin, B., Seitzinger, S., 2009. Composition of Dissolved Organic Nitrogen in Continental Precipitation Investigated by Ultra-High Resolution FT-ICR Mass Spectrometry. 43, 6950-6955.

Barsotti, F., Bartels-Rausch, T., De Laurentiis, E., Ammann, M., Brigante, M., Mailhot, G., Maurino, V., Minero, C., Vione, D., 2017. Photochemical formation of nitrite/nitrous acid (HONO) upon irradiation of nitrophenols in aqueous solution and in viscous secondary organic aerosol proxy. Environmental Science & Technology 51, 7486-7495.

Berto, S., De Laurentiis, E., Tota, T., Chiavazza, E., Daniele, P., Minella, M., Isaia, M., Brigante, M., Vione, D., 2016. Properties of the humic-like material arising from the photo-transformation of L-tyrosine. Science of The Total Environment 545-546, 434-444.

Bianco, A., Fabbri, D., Minella, M., Brigante, M., Mailhot, G., Maurino, V., Minero, C., Vione, D., 2015. New insights into the environmental photochemistry of 5-chloro-2-(2,4-dichlorophenoxy)phenol (triclosan): reconsidering the importance of indirect photoreactions. Water Res 72, 271-280.

Blessing, M., Schmidt, T.C., Dinkel, R., Haderlein, S.B., 2009. Delineation of Multiple Chlorinated Ethene Sources in an Industrialized Area-A Forensic Field Study Using. Environmental Science & Technology 43, 2701-2707.

Bodrato, M., Vione, D., 2014. APEX (Aqueous Photochemistry of Environmentally occurring Xenobiotics): A free software tool to predict the kinetics of photochemical processes in surface waters. Environmental science. Processes & impacts 16, 732-740.

Braslavsky, S., Acuña, A.U., Adam, W., Amat, F., Armesto, D., Atvars, T.D.Z., Bard, A., Bill, E., Björn, L.O., Bohne, C., Bolton, J., Bonneau, R., Bouas-Laurent, H., Braun, A., Dale, R., Dill, K., Döpp, D., Dürr, H., Chanon, M., Zachariasse, K., 2007. Glossary of Terms Used in Photochemistry, 3rd Edition (IUPAC Recommendations 2006). Pure and Applied Chemistry 79, 293-465.

Buchner, D., Jin, B., Ebert, K., Rolle, M., Elsner, M., Haderlein, S.B., 2017. Experimental Determination of Isotope Enrichment Factors - Bias from Mass Removal by Repetitive Sampling. Environ Sci Technol 51, 1527-1536.

Buth, J.M., Grandbois, M., Vikesland, P.J., McNeill, K., Arnold, W.A., 2009. Aquatic photochemistry of chlorinated triclosan derivatives: potential source of polychlorodibenzo-p-dioxins. Environ. Toxicol. Chem. 28, 2555-2563.

Buth, J.M., Ross, M.R., McNeill, K., Arnold, W.A., 2011. Removal and formation of chlorinated triclosan derivatives in wastewater treatment plants using chlorine and UV disinfection. Chemosphere 84, 1238-1243.

Chen, Z., Song, Q., Cao, G., Chen, Y., 2008. Photolytic degradation of triclosan in the presence of surfactants. Chemical Papers 62, 608-615.

Constantin, L.A., Nitoi, I., Cristea, N.I., Constantin, M.A., 2018. Possible degradation pathways of

triclosan from aqueous systems via TiO$_2$ assisted photocatalyis. Journal of Industrial and Engineering Chemistry 58, 155-162.

De Laurentiis, E., Minella, M., Sarakha, M., Marrese, A., Minero, C., Mailhot, G., Brigante, M., Vione, D., 2013a. Photochemical processes involving the UV absorber benzophenone-4 (2-hydroxy-4-methoxybenzophenone-5-sulphonic acid) in aqueous solution: Reaction pathways and implications for surface waters. Water research 47, 5943-5953.

De Laurentiis, E., Socorro, J., Vione, D., Quivet, E., Brigante, M., Mailhot, G., Wortham, H., Gligorovski, S., 2013b. Phototransformation of 4-phenoxyphenol sensitised by 4-carboxybenzophenone: Evidence of new photochemical pathways in the bulk aqueous phase and on the surface of aerosol deliquescent particles. Atmospheric Environment 81, 569-578.

Elsner, M., Imfeld, G., 2016. Compound-specific isotope analysis (CSIA) of micropollutants in the environment - current developments and future challenges. Current opinion in biotechnology 41, 60-72.

Elsner, M., Zwank, L., Hunkeler, D., Schwarzenbach, R.P., 2005. A new concept linking observable stable isotope fractionation to transformation pathways of organic pollutants. Environmental Science & Technology 39, 6896-6916.

Frank, R., Sanderson, H., Kavanagh, R., Kent Burnison, B., Headley, J., Solomon, K., 2010. Use of a (Quantitative) Structure–Activity Relationship [(Q)Sar] Model to Predict the Toxicity of Naphthenic Acids. Journal of toxicology and environmental health. Part A 73, 319-329.

García, S., Pinto, G., García-Encina, P., Irusta, R., 2014. Ecotoxicity and environmental risk assessment of pharmaceuticals and personal care products in aquatic environments and wastewater treatment plants. Ecotoxicology (London, England) 23, 1517-1533.

Gautam, P., Carsella, J.S., Kinney, C.A., 2014. Presence and transport of the antimicrobials triclocarban and triclosan in a wastewater-dominated stream and freshwater environment. Water Res 48, 247-256.

Hartenbach, A.E., Hofstetter, T.B., Tentscher, P.R., Canonica, S., Berg, M., Schwarzenbach, R.P., 2008. Carbon, Hydrogen, and Nitrogen Isotope Fractionation During Light-Induced Transformations of Atrazine. Environmental Science & Technology 42, 7751-7756.

Hofstetter, T.B., Schwarzenbach, R.P., Bernasconi, S.M., 2008. Assessing Transformation Processes of Organic Compounds Using Stable Isotope Fractionation. Environmental Science & Technology 42, 7737-7743.

Holder-Sandrik, S.L., P. Bilski, J.D. Pakulski, C.F. Chignell, 2000. Photogeneration of singlet oxygen and free radicals in dissolved organic matter isolated from the Mississippi and Atchafalaya River plumes. Marine Chemistry, 139-152.

Huang, Y., Kong, M., Westerman, D., Xu, E.G., Coffin, S., Cochran, K.H., Liu, Y., Richardson, S.D., Schlenk, D., Dionysiou, D.D., 2018. Effects of HCO3(-) on Degradation of Toxic Contaminants of Emerging Concern by UV/NO3(). Environ Sci Technol 52, 12697-12707.

Jiang, B., Liang, Y., Xu, C., Zhang, J., Hu, M., Shi, Q., 2014. Polycyclic aromatic hydrocarbons (PAHs) in ambient aerosols from Beijing: characterization of low volatile PAHs by positive-ion atmospheric pressure photoionization (APPI) coupled with Fourier transform ion cyclotron resonance. Environ Sci Technol 48, 4716-4723.

Jin, B., Rolle, M., 2014. Mechanistic approach to multi-element isotope modeling of organic contaminant degradation. Chemosphere 95, 131-139.

Jin, B., Rolle, M., 2016. Position-specific isotope modeling of organic micropollutants transformation

through different reaction pathways. Environ Pollut 210, 94-103.

Kliegman, S., Eustis, S.N., Arnold, W.A., McNeill, K., 2013. Experimental and Theoretical Insights into the Involvement of Radicals in Triclosan Phototransformation. Environmental Science & Technology 47, 6756-6763.

Kolpin, D., Furlong, E., Meyer, M., Thurman, E., Zaugg, S., B Barber, L., Buxton, H., 2002. Pharmaceuticals, Hormones, and Other Organic Wastewater Contaminants in U.S. Streams, 1999-2000: A National Reconnaissance. Environmental Science & Technology 36, 1202-1211.

Latch, D., L Packer, J., L Stender, B., VanOverbeke, J., A Arnold, W., McNeill, K., 2005. Aqueous Photochemistry of Triclosan: Formation of 2,4-Dichlorophenol, 2,8-Dichlorodibenzo-P-Dioxin, and Oligomerization Products. Environmental toxicology and chemistry / SETAC 24, 517-525.

Leresche, F., von Gunten, U., Canonica, S., 2016. Probing the Photosensitizing and Inhibitory Effects of Dissolved Organic Matter by Using N,N-dimethyl-4-cyanoaniline (DMABN). Environ Sci Technol 50, 10997-11007.

Lores, M., Llompart, M., Sanchez-Prado, L., Garcia-Jares, C., Cela, R., 2005. Confirmation of the formation of dichlorodibenzo-p-dioxin in the photodegradation of triclosan by photo-SPME. Analytical and Bioanalytical Chemistry 381, 1294-1298.

Lu, C.Y., Liu, Y. Y., 2002. Electron transfer oxidation of tryptophan and tyrosine by triplet states and oxidized radicals of flavin sensitizers: A laser flash photolysis study. Biochim. Biophys. Acta 1571, 71-76.

Madronich, S., 1987. Intercomparison of NO2 photodissociation and U.V. Radiometer Measurements. Atmospheric Environment (1967) 21, 569–578.

Mayo-Bean, K., Moran, K., Meylan, B., Ranslow, P., 2012. Methodology document for the ECOlogical Structure-Activity Relationship model (ECOSAR) class program., US-EPA, Washington DC, p. 46

Mekic, M., Brigante, M., Vione, D., Gligorovski, S., 2018a. Exploring the ionic strength effects on the photochemical degradation of pyruvic acid in atmospheric deliquescent aerosol particles. Atmospheric Environment 185, 237-242.

Mekic, M., Liu, J., Zhou, W., Loisel, G., Cai, J., He, T., Jiang, B., Yu, Z., Lazarou, Y.G., Li, X., Brigante, M., Vione, D., Gligorovski, S., 2019. Formation of highly oxygenated multifunctional compounds from cross-reactions of carbonyl compounds in the atmospheric aqueous phase. Atmospheric Environment 219.

Mekic, M., Loisel, G., Zhou, W., Jiang, B., Vione, D., Gligorovski, S., 2018b. Ionic-Strength Effects on the Reactive Uptake of Ozone on Aqueous Pyruvic Acid: Implications for Air-Sea Ozone Deposition. Environ Sci Technol 52, 12306-12315.

Net, S., Nieto-Gligorovski, L., Gligorovski, S., Temime-Rousell, B., Barbati, S., Lazarou, Y.G., Wortham, H., 2009. Heterogeneous light-induced ozone processing on the organic coatings in the atmosphere. Atmospheric Environment 43, 1683-1692.

Pan, H., 2008. A non-covalent dimer formed in electrospray ionisation mass spectrometry behaving as a precursor for fragmentations. Rapid Communications in Mass Spectrometry 22, 3555-3560.

Passeport, E., Zhang, N., Wu, L., Herrmann, H., Sherwood Lollar, B., Richnow, H.H., 2018. Aqueous photodegradation of substituted chlorobenzenes: Kinetics, carbon isotope fractionation, and reaction mechanisms. Water Res 135, 95-103.

Ratti, M., Canonica, S., McNeill, K., Erickson, P.R., Bolotin, J., Hofstetter, T.B., 2015. Isotope fractionation associated with the direct photolysis of 4-chloroaniline. Environ Sci Technol 49,

4263-4273.

Rayleigh, J.W.S., 1896. Theoretical considerations respecting the separation of gases by diffusion and similar processes. Philosophical Magazine and Journal of Science 42, 493-498.

Reuschenbach, P., Silvani, M., Dammann, M., Warnecke, D., Knacker, T., 2008. ECOSAR model performance with a large test set of industrial chemicals. Chemosphere 71, 1986-1995.

Sanchez-Prado, L., Llompart, M., Lores, M., Garcia-Jares, C., Bayona, J.M., Cela, R., 2006. Monitoring the photochemical degradation of triclosan in wastewater by UV light and sunlight using solid-phase microextraction. Chemosphere 65, 1338-1347.

Schmidt, T.C., Jochmann, M.A., 2012. Origin and Fate of Organic Compounds in Water: Characterization by Compound-Specific Stable Isotope Analysis, in: Cooks, R.G., Yeung, E.S. (Eds.), Annual Review of Analytical Chemistry, Vol 5. Annual Reviews, Palo Alto, pp. 133-155.

Sherwood Lollar, B., Slater, G.F., Sleep, B., Witt, M., Klecka, G.M., Harkness, M., Spivack, J., 2001. Stable carbon isotope evidence for intrinsic bioremediation of tetrachloroethene and trichloroethene at area 6, Dover Air Force Base. Environmental Science and Technology 35, 261-269.

Shi, Q., Pan, N., Long, H., Cui, D., Guo, X., Long, Y., Chung, K.H., Zhao, S., Xu, C., Hsu, C.S., 2012. Characterization of Middle-Temperature Gasification Coal Tar. Part 3: Molecular Composition of Acidic Compounds. Energy & Fuels 27, 108-117.

Sijm, D. T. H. M., Opperhuizen, A., 1988. Biotransformation, bioaccumulation and lethality of 2,8-dichlorodibenzo-p-dioxin: a proposal to explain the biotic fate and toxicity of PCDD's and PCDF's. Chemosphere 17, 83-99.

Singer, H., Müller, S., Tixier, C., Pillonel, L., 2003. Triclosan: Occurrence and Fate of a Widely Used Biocide in the Aquatic Environment: Field Measurements in Wastewater Treatment Plants, Surface Waters, and Lake Sediments. 36, 4998-5004.

Tixier, C., P Singer, H., Canonica, S., R Müller, S., 2002. Phototransformation of Triclosan in Surface Waters: A Relevant Elimination Process for This Widely Used BiocideLaboratory Studies, Field Measurements, and Modeling. Environmental Science & Technology 36, 3482-3489.

Vione, D., Albinet, A., Barsotti, F., Mekic, M., Jiang, B., Minero, C., Brigante, M., Gligorovski, S., 2019. Formation of substances with humic-like fluorescence properties, upon photoinduced oligomerization of typical phenolic compounds emitted by biomass burning. Atmospheric Environment 206, 197-207.

Vione, D., Fabbri, D., Minella, M., Canonica, S., 2018. Effects of the antioxidant moieties of dissolved organic matter on triplet-sensitized phototransformation processes: Implications for the photochemical modeling of sulfadiazine. Water Res 128, 38-48.

Vione, D., Maddigapu, P.R., De Laurentiis, E., Minella, M., Pazzi, M., Maurino, V., Minero, C., Kouras, S., Richard, C., 2011. Modelling the photochemical fate of ibuprofen in surface waters. Water Res 45, 6725-6736.

Vione, D., Scozzaro, A., 2019. Photochemistry of Surface Fresh Waters in the Framework of Climate Change. Environ Sci Technol 53, 7945-7963.

Vogt, C., Cyrus, E., Herklotz, I., Schlosser, D., Bahr, A., Herrmann, S., Richnow, H.-H., Fischer, A., 2008. Evaluation of Toluene Degradation Pathways by Two-Dimensional Stable Isotope Fractionation. Environmental Science & Technology 42, 7793-7800.

Vogt, C., Dorer, C., Musat, F., Richnow, H.H., 2016. Multi-element isotope fractionation concepts to characterize the biodegradation of hydrocarbons - from enzymes to the environment. Curr Opin

Biotechnol 41, 90-98.

Wenk, J., Canonica, S., 2012. Phenolic antioxidants inhibit the triplet-induced transformation of anilines and sulfonamide antibiotics in aqueous solution. Environ Sci Technol 46, 5455-5462.

Wu, J.L., Ji, F., Zhang, H., Hu, C., Wong, M.H., Hu, D., Cai, Z., 2019. Formation of dioxins from triclosan with active chlorine: A potential risk assessment. J Hazard Mater 367, 128-136.

Wu, L., Chládková, B., Lechtenfeld, O., Lian, S., Schindelka, J., Herrmann, H., Richnow, H., 2018. Characterizing chemical transformation of organophosphorus compounds by (13)C and (2)H stable isotope analysis. 615, 20-28.

Zhang, N., Schindelka, J., Herrmann, H., George, C., Rosell, M., Herrero-Martín, S., Klán, P., Richnow, H., 2015. Investigation of Humic Substance Photosensitized Reactions via Carbon and Hydrogen Isotope Fractionation. 49, 233-242.

Zhang, S., Chen, J., Xie, Q., Shao, J., 2011. Comment on "Effect of dissolved organic matter on the transformation of contaminants induced by excited triplet states and the hydroxyl radical". Environ Sci Technol 45, 7945-7946; author reply 7947-7948.

Zhao, J.L., Zhang, Q.Q., Chen, F., Wang, L., Ying, G.G., Liu, Y.S., Yang, B., Zhou, L.J., Liu, S., Su, H.C., Zhang, R.Q., 2013. Evaluation of triclosan and triclocarban at river basin scale using monitoring and modeling tools: implications for controlling of urban domestic sewage discharge. Water Res 47, 395-405.

Zhao, S., Ma, H., Wang, M., Cao, C., Xiong, J., Xu, Y., Yao, S., 2010. Study on the mechanism of photo-degradation of p-nitrophenol exposed to 254 nm UV light. J Hazard Mater 180, 86-90.